The described concept can be extended to noise-shaping of any order. The only requirement is to make the signal transfer function *STF* exactly equal to 1, without changing the noise transfer function.

In practice, the cancellation of u and v will not be perfect. As indicated before, v is an estimate of u, and its accuracy depends on the matching of electrical parameters. Hence, there will be some residual signal component in e and at the outputs of the integrators, but this will be normally negligible.

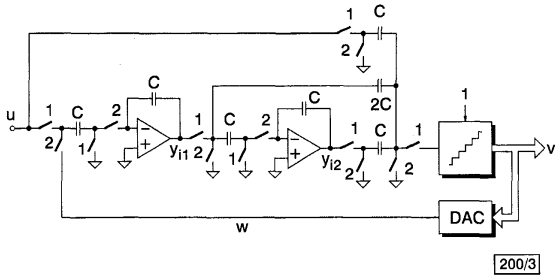

Fig. 3 *Circuit diagram implementation*

Circuit level implementation: The forward paths in Fig. 2 can be implemented by connecting a passive switched-capacitor network to the input of the quantiser. This network can also be used to apply a dither signal, an essential feature at low oversampling ratios. A complete circuit diagram, shown in single-ended form for simplicity, is shown in Fig. 3.

In practice, there will always be a small delay between u and v. However, as it will be explained next, this delay can be cancelled. The input signal u is sampled by a non-inverting (delaying) SC branch during phase Φ_1, and integrated during phase Φ_2 when the feedback signal w is entered using an inverting (non-delaying) branch in the DAC. The quantiser evaluates the input signal at the end of Φ_1, and provides the feedback signal during Φ_2. The end result is that there is no effective delay between the input signal sample which the first integrator is processing and the feedback signal associated with that sample.

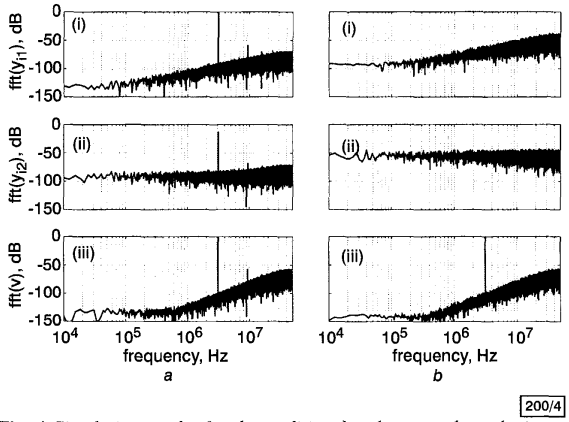

Fig. 4 *Simulation results for the traditional and proposed topologies*

a Traditional topology
b Proposed topology
(i) spectrum of $y_{i1}(n)$
(ii) spectrum of $y_{i2}(n)$
(iii) spectrum of $v(n)$

Simulation results: The proposed structure, shown in Fig. 2, was simulated with MATLAB and its linearity performance compared with that of the traditional scheme (Fig. 1). The model used for the integrators incorporated a nonlinear opamp input-output transfer curve, in the form of a hyperbolic tangent with a maximum gain of 50 dB.

Both structures were simulated with a sampling frequency of 100 MHz, a 6 bit quantiser, and with a uniformly distributed random dither signal. The sine-wave input signal u had an amplitude 0.9 V (for a voltage reference of 1 V) and a frequency 3.125 MHz. Scaling factors were included in each structure to ensure that the integrator output voltages were comparable.

The spectra of the signals $y_{i1}(n)$, $y_{i2}(n)$ and $v(n)$ for the two topologies were computed using 32768-point FFTs, and are shown in Fig. 4. The traditional topology shows the presence of input signal at the integrator outputs, together with harmonics created due to the nonlinear function. The modulator output v shows a third harmonic with an amplitude of −57.3 dBc. The proposed topology shows only shaped quantisation noise at these nodes (and therefore no harmonics of the input signal), and so the modulator had an undistorted output.

Note that both simulations show an increased noise floor compared to the ideal response. Part of this is caused by finite opamp gain. The other part is caused by the nonlinearities, which fold energy from high-frequencies down into the signal band. However, due to the absence of signal components, the proposed topology has a lower noise floor.

Additional remarks: The nonlinearities of the DAC in the feedback path are not addressed by the proposed topology. Analogue mismatch correction [3] can be used to linearise the DAC independently of the oversampling ratio.

The proposed structure can be used as the first stage of a cascaded ΔΣ structure. Since the quantisation noise is processed separately from the input signal, it can be tapped directly from the output of the second integrator, y_{i2}. This configuration has the added advantage of cancelling the quantiser (ADC) nonlinearities in the output v.

Conclusions: A ΔΣ topology with reduced sensitivity to nonlinear opamps has been described. The technique is effective for any oversampling ratio, and can be applied to any modulator order.

Acknowledgments: The authors would like to thank the NFS Center for the Design of Analog and Digital Integrated Circuits for support.

20 April 2001
Electronics Letters Online No: 20010542
DOI: 10.1049/el:20010542

J. Silva, U. Moon and G.C. Temes (*Department of Electrical and Computer Engineering, Owen Hall, Oregon State University, Corvallis, OR 97331-3211, USA*)

J. Steensgaard (*Department of Electrical Engineering, Columbia University, New York, NY 10027, USA*)

References

1 STEENSGAARD, J.: 'Nonlinearities in SC delta-sigma A/D converters'. IEEE Int. Conf. Electronics, Circuits and Systems, Lisbon, Portugal, 1998, Vol. 1, pp. 355–358

2 STEENSGAARD, J.: 'High-performance data converters'. PhD thesis, The Technical University of Denmark, Department of Information Technology, 8 March, 1999, pp. 170–171

3 MOON, U., SILVA, J., STEENSGAARD, J., and TEMES, G.C.: 'A switched-capacitor DAC with analogue mismatch correction', *Electron. Lett.*, 1999, **22**, pp. 1903–1904

Iterative FEM for characterising radiating slot in broad wall of rectangular waveguide

Jongkuk Park, Jungwon Lee, Heeduck Chae and Sangwook Nam

It is shown that the iterative finite element method with the radiation-type boundary condition can give an efficient and accurate solution to the radiation problem. The proposed method is applied to the characterisation of a radiating slot on the broad wall of a rectangular waveguide. The result is compared with those of other conventional methods, and shows a good agreement.

Introduction: Recently an efficient iterative finite element method (iterative FEM) has been proposed [1], applied to a two-dimensional scattering problem [2], and extended to the characterisation

of three-dimensional discontinuities in a rectangular waveguide [3]. In the above cases, when there is a small number of meshes around a scatterer, a finite element method has been shown to give good results. However, the Dirichlet condition used in the above method has been found to be unsuitable for characterising the scattering caused by resonant slots or large cavities due to the internal resonance problem. Thus, to eliminate this phenomenon, a radiation-type boundary condition has been proposed [4] and extended to a three-dimensional scattering problem [5].

In this Letter, the iterative FEM is applied to the characterisation of a radiating slot, which is used widely as an element of waveguide slot array antennas. This radiating slot is approximately half a wavelength in size, which means that internal resonance is liable to occur. Therefore, the radiation-type boundary condition is incorporated with this method to prevent such internal resonance.

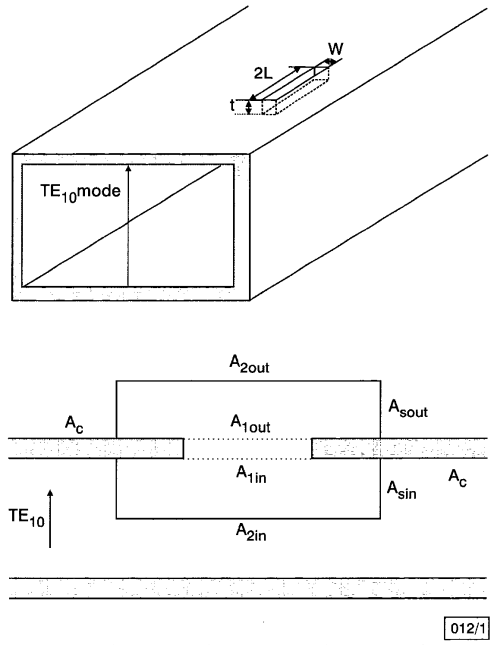

Fig. 1 *Geometry of radiating slot in rectangular waveguide*

Theory: Fig. 1 shows the geometry of a slot on a rectangular waveguide and the definition of surfaces used in the proposed method. As shown in Fig. 1, the volume enclosed by A_{2in}, A_{2out}, A_c will be discretised into finite elements, and so A_{2in}, A_{2out} denote the boundary surfaces where the finite element meshes are terminated. On these boundary surfaces A_{2in} and A_{2out}, each boundary condition is imposed as follows:

$$\begin{aligned} \hat{n} \times \nabla \times \vec{E} + j\beta_{10} \hat{n} \times \hat{n} \times \vec{E} &= \vec{U}_{in} \quad \text{on } A_{2in} \\ \hat{n} \times \nabla \times \vec{E} + jk_0 \hat{n} \times \hat{n} \times \vec{E} &= \vec{U}_{out} \quad \text{on } A_{2out} \end{aligned} \tag{1}$$

With the given boundary conditions, the electric field in the volume and on the boundary surfaces can be calculated by seeking the stationary point of the functional given by

$$\begin{aligned} F(\vec{E}) = \frac{1}{2} \int_V \frac{1}{\mu_r} (\nabla \times \vec{E}) \cdot (\nabla \times \vec{E}) - k_0^2 \varepsilon_r \vec{E} \cdot \vec{E}\, dv \\ + \frac{j\beta_{10}}{2} \int_{A_{2in}} (\hat{n} \times \vec{E}) \cdot (\hat{n} \times \vec{E})\, ds \\ + \frac{jk_0}{2} \int_{A_{2out}} (\hat{n} \times \vec{E}) \cdot (\hat{n} \times \vec{E})\, ds \\ + \int_{A_{2in}} \vec{E} \cdot \vec{U}_{in}\, ds + \int_{A_{2out}} \vec{E} \cdot \vec{U}_{out}\, ds \end{aligned} \tag{2}$$

Initially, it is assumed that only the TE_{10} mode exists inside the rectangular waveguide and there is no field outside. Thus, $\vec{U}_{out}$ in eqn. 1 is equal to zero and $\vec{U}_{in}$ in eqn. 1 can be obtained easily from solving the TE_{10} mode inside the rectangular waveguide. Using the typical finite element procedure, we can calculate the electric field inside the volume. However, this field is not the accurate final solution we are seeking since the field on the boundary is not a real solution but an assumed one. To obtain a more accurate solution, we update the boundary field using the equivalent magnetic current, which is given by the field calculated on slot surfaces A_{1in} and A_{1out}. In this procedure, the appropriate Green function should be used in the updating integral equation. Outside the waveguide, the simple free-space Green function is employed and so the updated $\vec{U}_{out}$ can be easily calculated. However, inside the rectangular waveguide, the waveguide Green function, represented by the infinite series, which converges very slowly, should be used. Since it is almost impossible to calculate this waveguide Green function as it is, its series form is accelerated so that it converges fast enough to calculate it numerically using the Poisson summation formula and the Kummer transform [6]. Although the infinite series is accelerated so that it itself rapidly converges, the numerical integration for updating the boundary fields is still a time-consuming procedure. However, this numerical integration is performed only once at the first iteration since its value is stored in a matrix form and this matrix is invariant during the iterations. This property makes the proposed method very efficient. With these updated boundary fields, the typical finite element procedure is performed again. The system matrix in this procedure is highly sparse and invariant during the iterations. In order to exploit this property, the bandwidth of the system matrix is reduced by the Gibbs-Poole-Stockmeyer algorithm [7], and then the banded matrix is decomposed into the LDL^T form. This decomposition is a little time-consuming, but it is performed only once since the matrix is invariant during the iterations. Therefore, in the subsequent iterations, only fast forward and backward substitutions are required to obtain the finite element solution.

After a few iterations, the solution converges within a given error criterion. The other physical quantities such as S-parameters are calculated using the final field solution.

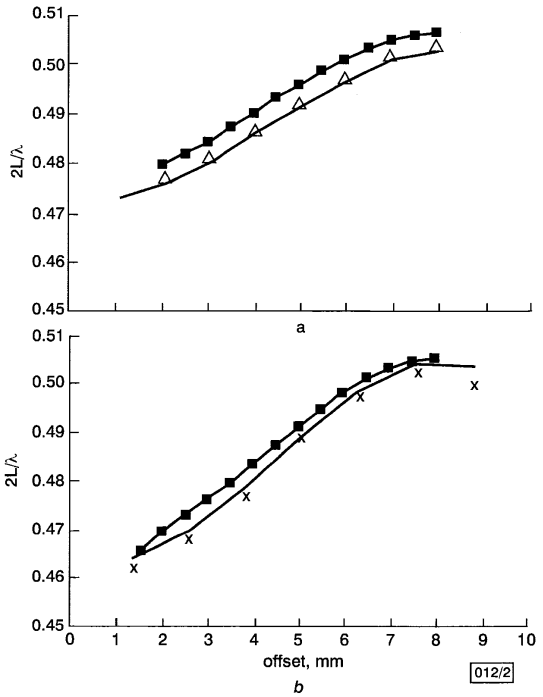

Fig. 2 *Resonant lengths of longitudinal slot on broad wall of rectangular waveguide (WR-90) against offset from centreline*

w = 1.59 mm, *f* = 9.375 GHz
a *t* = 1.27 mm
—■— proposed method
——— result from [8]
△ result from [9]
b *t* = 0.38 mm
—■— proposed method
——— result from [8]
× measured [8]

Numerical results: Based on the theory described above, a longitudinal slot in a rectangular waveguide was characterised to show the validity of the proposed method. WR-90 was selected as the

rectangular waveguide. In Fig. 1, $2L$, w, t denote the resonant length, the width, and the thickness of a longitudinal slot, respectively. Fig. 2 shows the normalised resonant length of a slot according to offset from the centreline on the broad wall with slot thickness as the parameter at a fixed frequency. The results agree well with those of other conventional methods [8, 9] with an error of less than 1%.

Conclusion: An application of iterative FEM has been extended successfully to the characterisation of a radiating slot in a rectangular waveguide. Comparing the result with other conventional solutions, we have shown that this method gives a good and efficient solution.

Acknowledgment: This work was supported by the Brain Korea 21 Project.

9 April 2001
Electronics Letters Online No: 20010526
DOI: 10.1049/el:20010526

Jongkuk Park, Jungwon Lee, Heeduck Chae and Sangwook Nam (*School of Electrical Engineering, Seoul National University, Seoul, Korea*)

References

1 ROY, T., SARKAR, T.K., DJORDJEVIC, A.R., and SALAZA, M.: 'Hybrid method for terminating the finite element mesh (electrostatic case)', *Microw. Opt. Technol. Lett.*, 1995, **8**, (6), pp. 282–287
2 ROY, T., SARKAR, T.K., DJORDJEVIC, A.R., and SALAZA, M.: 'Hybrid method solution of scattering by conducting cylinders (TM case)', *IEEE Trans. Microw. Theory Tech.*, 1996, **MTT-44**, (12), pp. 2145–2151
3 PARK, J., CHAE, H., and NAM, S.: 'Efficient hybrid method for characterisation of arbitrary-shaped discontinuities in rectangular waveguide', *Electron. Lett.*, 1999, **35**, (14), pp. 1170–1171
4 ALFONZETTI, S., BORZI, G., and SALERNO, N.: 'Iteratively-improved robin boundary conditions for the finite element solution of scattering problems in unbounded domains', *Int. J. Numer. Meth. Eng.*, 1998, **42**, pp. 601–629
5 PARK, J., CHAE, H., and NAM, S.: 'Study of efficient FEM-based iteration method for open region problem and its application to scattering from a three-dimensional cavity-backed aperture', *Electron. Lett.*, 2000, **36**, (18), pp. 1529–1530
6 AHN, B.C.: 'Moment method analysis of a narrow wall inclined slot on a rectangular waveguide'. PhD dissertation, University of Mississippi, Oxford 1992
7 GIBBS, N.E., POOLE, W.G., Jr., and STOCKMEYER, P.K.: 'An algorithm for reducing the bandwidth and profile of a sparse matrix', *SIAM J. Numer. Anal.*, 1976, **13**, (2), pp. 236–250
8 JOSEFSSON, L.G.: 'Analysis of longitudinal slots in rectangular waveguides', *IEEE Trans. Antennas Propag.*, 1987, **AP-35**, (12), pp. 1351–1357
9 KHAC, T.B.: 'A study of some slot discontinuities in rectangular waveguides'. PhD dissertation, Monash University, Australia, Nov. 1974

Cascaded Raman fibre laser for stable dual-wavelength operation

Do Il Chang, Dong Sung Lim, Min Yong Jeon, Kyong Hon Kim and Taesang Park

The authors have demonstrated a stable and tunable dual-wavelength Raman fibre laser, which can be used as a pump source for a hybrid type and gain controlled C- and L-band distributed Raman and lumped erbium-doped fibre amplifier. Intensity and wavelength tuning of the two lasing modes at 1480 nm and 1500 nm are achieved by tuning one and both of the fibre gratings used in the laser cavity, respectively.

Introduction: In Raman amplifiers pumped by several laser sources with different wavelengths, the gain profile is described approximately by a linear superposition of each gain induced by an individual pump [1]. Multi-wavelength pumping, therefore, is an attractive method for expanding the gain bandwidth in Raman amplifiers. Multi-wavelength lasers have been realised through multiplexing of laser diodes [2] or fibre lasers [3]. These techniques, however, need several pump lasers and low loss pump combiners, which make the laser system complicated and expensive.

Previously we described a dual-wavelength Raman laser based on a ring type intracavity with two pairs of fibre gratings [4]. In this Letter, we demonstrate a modified cascaded Raman fibre laser, which generates a more stable dual-wavelength. It has two independent resonators to prevent interference between the two wavelengths. Stable and electronically tunable dual wavelength laser operation of this device makes it highly attractive, especially for the active gain control of a Raman amplifier.

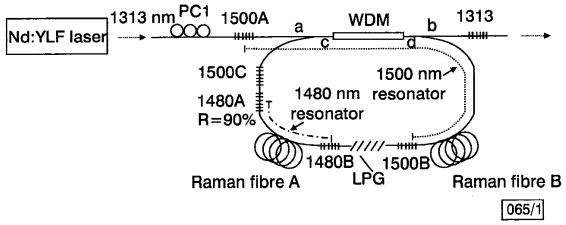

Fig. 1 *Schematic diagram of cascaded Raman fibre laser*

All fibre Bragg gratings have reflectivity, R, > 99% except 1480A (R = 90%)

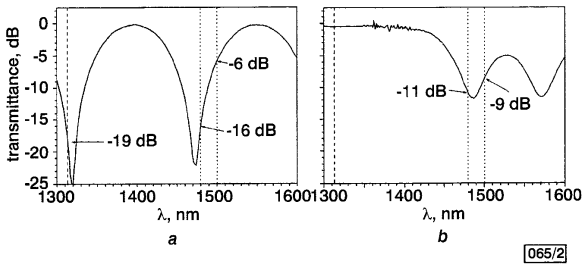

Fig. 2 *Transmission spectra of WDM and LPG*

a WDM
b LPG

Experimental apparatus: A schematic diagram of the laser setup is shown in Fig. 1. The laser is pumped by an Nd:YLF laser operating at 1313 nm. The pump power is coupled into the active Raman fibre through port a to port d of the WDM and then converted into a first-order Stokes wavelength. Since the Raman frequency shift in the silica fibre is around 440 cm^{-1}, conversions from 1313 to 1480 nm or 1500 nm occurs through cascaded Raman scattering up to the second order via the first intermediate Stokes order. The intra-cavity consisting of the WDM coupler resonates at the first-order Stokes wavelength.

Dual-second-order Stokes wavelengths are separately generated in the 1480 nm and 1500 nm resonator. As the active Raman medium, a 120 m length of dispersion compensating fibre (DCF, Raman fibre A) for the 1480 nm resonator and a 220 m length of DCF (Raman fibre B) for the 1500 nm resonator are used. The unconverted pump power emerging from the loop (from port c to port b) is reflected backward by the fibre Bragg grating, 1313 nm, and re-coupled into the Raman fibre.

Fig. 2*a* depicts the transmittance spectrum profile between port c and port d of the WDM coupler. The dashed line indicates the pump wavelength at 1313 nm, while the two dotted lines indicate the desired laser output wavelengths at 1480 nm and 1500 nm, respectively. The WDM coupler is designed to have maximum transmission for the first-order Stokes wavelength around 1396 nm and minimum transmission for the pump wavelength at 1313 nm and second-order Stokes wavelength at 1480 nm. The measured transmittance of the fabricated WDM is 1% (–19 dB) at 1313 nm and 3% (–16 dB) at 1480 nm. It also provides 25% (–6 dB) transmittance at 1500 nm, meaning 75% transmittance between port a and port d.

To generate the second-order Stokes wavelength at 1480 nm, 1480A (R = 90%) and 1480B (R > 99%) were used as an output